Centrifugation-based separation of triangular silver nanoplates from multi-shaped colloidal silver nanoparticles for fabrication of surface-enhanced Raman-scattering substrates

[1] Phetsahai A., [2] Eiamchai P., [1*] Thamaphat K. and [1] Limsuwan P.

[1] Green Synthesis and Application Laboratory, Applied Science and Engineering for Social Solution Research Unit, Department of Physics, Faculty of Science, King Mongkut's University of Technology Thonburi, Bangkok 10140, Thailand kheamrutai.tha@kmutt.ac.th

[2] Opto-Electrochemical Sensing Research Team, National Electronics and Computer Technology Center (NECTEC), National Science and Technology Development Agency (NSTDA), Pathum Thani 12120, Thailand

Abstract. We synthesize and separate triangular silver nanoplates (TSNPs) from a mixture of colloidal silver nanoparticles of different shapes and sizes, aiming at fabrication of substrates for a surface-enhanced Raman scattering (SERS). The TSNPs are successfully synthesized via a photochemical process involving Ag nanoseeds. This is confirmed by the UV-visible spectroscopy and transmission electron-microscopy analyses. Centrifugation-based separation techniques are employed to isolate the TSNPs and minimize the other nanoparticle morphologies, thus resulting in a good SERS performance. The separated TSNPs manifest a remarkable sensitivity, with the detection limit amounting to 10^{-12} M in the case of Rhodamine 6G molecules. A linear relationship between the Rhodamine 6G concentration and the Raman-peak intensity demonstrates a great potential of our SERS technique. Hence, our study combines a successful synthesis and separation of the TSNPs with demonstration of their efficient SERS performance. The latter offers new possibilities for the ultrasensitive trace-level detection of substances. These findings contribute to the development of reliable SERS measurements and the advance in the field of nanomaterial-based sensing techniques.

1. Introduction

Raman spectroscopy is a widely employed analytical technique that provides valuable insights into molecular structures and interactions. It reveals chemical compositions and structural characteristics of molecules by measuring inelastic scattering of photons. In spite of many advantages, a conventional Raman spectroscopy encounters limitations in sensitivity, in particular when detecting analytes at low concentrations or with weak Raman signals [1, 2]. To overcome this constraint, a surface-enhanced Raman scattering (SERS) has emerged as an exceptional technique that offers remarkable sensitivity and versatility. These features make it highly appealing for a diverse range of applications, including environmental monitoring, biomedical diagnostics and forensic analysis [3–5].

The SERS achieves substantial amplification of the Raman signals from analyte molecules, which can reach several orders of magnitude. This effect is due to interaction of the molecules

with the noble-metal nanostructures that possess unique plasmonic properties. Hence, the extraordinary sensitivity enhancement arises from the phenomenon of localized surface-plasmon resonance peculiar for these noble-metal nanostructures. This phenomenon occurs due to a strong coupling between the incident light and the collective oscillations of conduction electrons at a metal surface, which results in a significant enhancement of the local electromagnetic field surrounding a nanostructure [6, 7]. In its turn, the enhanced electromagnetic field interacts with nearby molecules, thus intensifying their Raman-scattering signal through an electromagnetic-enhancement mechanism [8]. The efficiency of the effect depends on many factors such as a shape, a size and composition of noble-metal nanostructures, as well as precise positions of analyte molecules inside electromagnetic hotspots generated by nanostructures [6, 9]. As a consequence, fabrication of SERS-active substrates and accurate design of SERS measurements play a vital role.

Colloidal SERS-active substrates have gained significant popularity due to ease of their fabrication, compositional versatility, large surface area and strong ability to form enhancing hotspots [10–12]. Among various noble-metal nanostructures explored as colloidal SERS-active substrates, silver nanoparticles (AgNPs) have gained substantial attention of researchers due to their exceptional plasmonic properties, including a strong localized surface-plasmon resonance and a high scattering efficiency in the visible range [13, 14]. In particular, triangular silver nanoplates (TSNPs) offer distinct advantages over other nanostructures due to their sharp corners and edges, which create localized electromagnetic hotspots and promote efficient light–matter interactions [6, 15]. These unique features enable stronger coupling with the analyte molecules and so strong Raman-signal amplification. Additionally, the abundance of crystal facets (111) in the TSNPs enhances their surface reactivity and facilitates stronger chemical interactions with the analyte molecules [16, 17].

The colloidal TSNPs have been synthesized using various methods that encompass physical, chemical and bio-based processes [18]. Among these approaches, a chemical reduction represents the most commonly employed method, which utilizes organic and/or inorganic reducing agents to generate nanoseeds. The nanoseeds are subsequently transformed into triangular nanoplates via different light-induced reactions [10, 11, 19–23], which is known as a seed-mediated photochemical method. Achieving of a high yield of the TSNPs in this method, which is suitable for the satisfactory SERS performance, involves subjecting Ag nanoseeds to light irradiation with specific durations (typically from 2 to 5 h). The optimal irradiation time depends on various parameters, including the light wavelength, the intensity, the reaction temperature, the seed concentration and the characteristics of a surrounding medium [6, 7, 10, 11, 17, 24–26].

It is important to note that, besides of the TSNPs, the self-assembled Ag nanostructures obtained under photo-irradiation include also a mixture of nanoparticles with polydispersity in terms of their shapes and sizes, including nanospheres, nanowires and irregularly shaped nanoparticles [23, 27]. Heterogeneity in the nanoparticle morphology poses challenges in achieving a consistent and reproducible SERS performance. The variations in the electromagnetic-field enhancement across a sample, which results from different shapes and sizes of nanoparticles, can lead to variable SERS signals. This potentially impacts both reproducibility and reliability of the SERS measurements. This is why separation of the TSNPs from the mixture of different nanoparticles becomes crucial if one wishes to ensure a consistent and reliable SERS performance and a precise and meaningful analysis of the data.

To address these challenges, we suggest optimizing the synthesis parameters and implementing a centrifugation-based separation technique in order to isolate the TSNPs and

minimize the presence of other multi-shaped AgNPs. This approach aims to improve the SERS performance by achieving a more uniform and controllable plasmonic response. In this work, we present a comprehensive study focused on the synthesis of TSNPs through photoconversion of Ag nanoseeds. The photoconversion process involves exposing Ag nanoseeds to light emitted by a high-pressure sodium lamp with the wavelength 589 nm (corresponding to the photon energy 2.1 eV) and the duration time of only 1 h. Subsequently, we vary the centrifugation time as a critical parameter in the centrifugation-based separation process, to obtain the TSNPs manifesting the highest SERS performance. The SERS activity of the separated particles at different centrifugation times has been evaluated using rhodamine 6G (R6G) as a target molecule with colloidal SERS-active substrates, without drop casting. This approach offers many advantages such as enhanced sensitivity, homogeneous particle distribution, ease of handling, and stability [17]. Additionally, we investigate the morphology and the plasmonic behaviour of the colloidal AgNPs before and after their separation. Our findings have significant implications for the advances of SERS techniques.

2. Materials and methods

2.1. Preparation of TSNPs using the photochemical method

Preparation of self-assembled Ag nanostructures in the shape of triangular nanoplates was based on a photochemical method and involved two main steps. First, Ag nanoseeds were synthesized using a conventional chemical reduction method with a customized recipe. A 10 mM silver nitrate ($AgNO_3$) solution was prepared by dissolving 99.9% $AgNO_3$ (POCH, Poland) in deionized water, while a 300 mM solution of trisodium citrate dihydrate ($Na_3C_6H_5O_7 \cdot 2H_2O$, from Ajex Finechem, Australia) was prepared by dissolving the compound in deionized water. The $AgNO_3$ (0.75 mL) and trisodium citrate dihydrate (0.75 mL) solutions were added to 72.75 mL of deionized water, which was followed by stirring of the mixture at the rate 433 rpm for 30 min. Then 37.5 µL of the 8 mM solution of sodium borohydride ($NaBH_4$, QReC, New Zealand) was slowly added to the mixture in a dropwise manner, while stirring continued for additional 2 min. The change in the colour to light yellow confirmed a formation of Ag nanoseeds, which were then stored in the dark at 4ºC for 2 h.

As the next step, self-assembled colloidal AgNPs were synthesized with a photochemical process. A 20 mL portion of the Ag-nanoseed solution was collected and transferred to a transparent vial. The solution was then exposed to the visible light with the wavelength 589 nm for 1 h. Two high-pressure sodium lamps (Luna, SC735) were used as light sources. They provided the irradiance of approximately 130 mW/cm^2. The reaction temperature was carefully maintained at a constant value, 39.1±0.6°C, throughout the overall photochemical-synthesis process.

The optical and general physical properties of the solutions obtained before and after light irradiation were analyzed using a UV-visible spectroscopy and a transmission electron microscopy (TEM). The properties of the solutions obtained before and after light irradiation were compared in order to assess any changes in the self-assembled colloidal AgNPs. Furthermore, the self-assembled colloidal AgNPs obtained after light irradiation were subjected to centrifugation to determine experimentally the optimal centrifugation time needed for obtaining the TSNPs with high SERS performance.

2.2. Separation of TSNPs by varying the centrifugation time

Separation of the TSNPs from the colloidal mixture was achieved through centrifugation. The colloidal AgNPs, which become self-assembled via the photoconversion process, were transferred

to four microcentrifuge tubes, where each tube contained 1.5 mL of the colloidal solution. Then the tubes were centrifuged at the speed of 14000 rpm with varying durations (5, 10, 15 and 20 min), using a high-speed microcentrifuge (UGAIYA, M16). After each centrifugation, a bright yellow supernatant containing unbound nanoparticles was carefully separated from the sediment, using a syringe. The sediment observed as a concentrated dark blue solid-like deposit at the bottom of each tube, was then dissolved in 9 mL of deionized water. The resulting solution was thoroughly mixed with a vortex for 10 s to ensure its homogeneity. The optical and general physical properties of the solutions obtained from both sediment and supernatant were studied at each centrifugation time. Furthermore, the sediment solutions were stored in a dark environment at the temperature 4ºC until they were utilized for subsequent SERS measurements.

2.3. Experimental details of SERS

The SERS experiments were conducted to assess the enhancement of Raman signals from analyte molecules. Two types of substrates were used: the self-assembled colloidal AgNPs after light exposure (before centrifugation) and the sediment solutions obtained at each centrifugation time. The experimental procedures of the SERS measurements are detailed in Fig. 1 and described below.
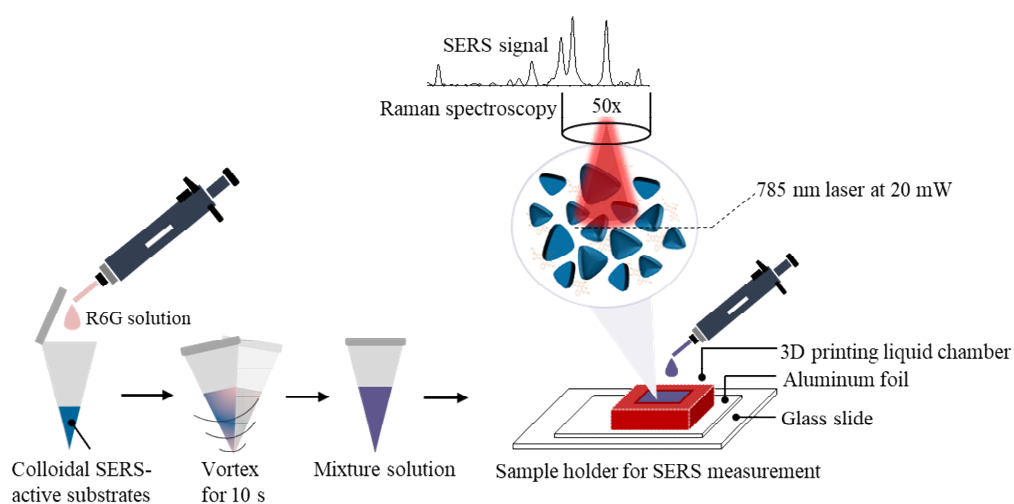

Fig. 1. Illustration of our SERS-measurement method.

To prepare samples for the SERS measurements, colloidal SERS-active substrates were thoroughly mixed with R6G (the dye content 99%; Sigma-Aldrich, Thailand) which served as a testing analyte. A 10^{-4} M solution of R6G was prepared and the colloidal substrates and R6G were mixed according to the volume ratio 1:1 for 10 s, using a vortex to ensure homogeneity. Subsequently, 200 μL of the resulting mixture was pipetted into a cost-effective liquid chamber with the dimensions $3{\times}5{\times}5$ mm^3. This liquid chamber was designed specifically for this study, using a 3D printing technology. It was mounted onto a glass slide covered with an aluminium foil. The use of this custom liquid chamber facilitated efficient containment of a sample and its subsequent analysis.

The Raman spectra were recorded using a Renishaw inVia Raman spectrometer equipped with a 50$^{\times}$ objective lens. The excitation wavelength was set at 785 nm, and the laser light (the maximum output power 20 mW) was focused on the middle height of the liquid chamber. The Raman signals were collected at a single point with a 10-second acquisition time and three

accumulations. This experimental setup provided precise Raman spectral measurements and enabled the capture of vibrational information from the analyte molecules. The selected excitation wavelength and the acquisition parameters chosen by us provided optimal signal-to-noise ratios, which contributed to reliable and reproducible data acquisition.

It is important to highlight that the above experimental details were consistently applied in all the SERS measurements conducted throughout this study. This standardized approach ensured the comparability and validity of the results obtained. Finally, the Raman enhancement factor was calculated and our further studies were conducted on the colloidal SERS-active substrates that revealed the highest SERS activity, with a specific focus on their ability to detect R6G in a dilution series.

2.4. Characterization methods

The characterization methods utilized in this study involved the TEM and the UV-visible spectroscopy. For the TEM analysis, a JEOL JEM-2100 transmission electron microscope was employed to examine the morphology of our samples. A drop of the solution was deposited onto a carbon-coated copper grid and left to air-dry at the room temperature. Subsequently, the prepared grid was inserted into a TEM chamber and the appropriate images were acquired under the acceleration voltage 120 kV. The TEM images obtained in this manner were carefully analyzed to determine the sizes, the shapes and the distribution of the nanoparticles. The sizes of the particles were measured with SemAfore 5.2 software.

The UV-visible spectroscopy was based on an Avantes AvaSpec-EDU spectrophotometer. It was employed to investigate the optical properties of our samples. The solution with the volume 3 mL was placed into a quartz cuvette and the absorbance spectrum was recorded inside the wavelength range 350–850 nm. This spectrum provided valuable insights into the plasmonic resonance and the absorption characteristics of the nanoparticles.

The characterization methods mentioned above were consistently applied throughout all the studies to ensure an accurate and reliable analysis of our materials. The TEM analysis allowed for visualization and determination of morphology of the nanoparticles, while the UV-visible spectroscopy provided the information on their optical properties. By combining these techniques, we achieved a comprehensive understanding of the structural and optical characteristics of the nanoparticles.

3. Results and discussion

3.1. Self-assembly of silver nanoparticles under visible-light exposure

The AgNPs which included the TSNPs have been successfully synthesized through the two-step process involving a generation of Ag nanoseeds and their subsequent transformation into TSNPs with the photochemical process. The use of $AgNO_3$, $NaBH_4$ and $Na_3C_6H_5O_7$ as important chemical precursors in the synthesis process enables a controllable formation of the Ag nanoseeds with small sizes and initial morphology [23, 24, 27]. The generation of the Ag nanoseeds begins with the reduction of silver ions (Ag^+) obtained from $AgNO_3$, which is facilitated by a presence of citrate ions in $Na_3C_6H_5O_7$. The citrate ions act as a protective layer on the surfaces of Ag^+, thus preventing efficiently their agglomeration and ensuring their stability. This protective layer plays a vital role in promoting a controlled growth of the nanoseeds. The addition of $NaBH_4$ as a reducing agent initiates the reduction reaction in a slow and controlled manner, which converts Ag^+ into silver atoms (Ag^0) and leads to formation of the nanoseeds [23]. A precise combination of these chemical precursors with a controlled reduction process results in the successful synthesis of the Ag nanoseeds with desired properties [18].

The efficiency of the synthesis process is confirmed by observation of a bright yellow colour in the resulting solution, as illustrated in Fig. 2a. This colour change can be attributed to the surface-plasmon absorption characteristics of the spherical Ag nanoseeds (see Fig. 2a). The UV-visible spectrum (red line) manifests a distinct peak at approximately 398 nm (see Fig. 2b). This indicates a presence of dipole plasmon resonance in the Ag nanoseeds [28]. A presence of this peak in the UV-visible spectrum supports further a successful formation of the Ag nanoseeds and validates their spherical morphology. Additionally, the TEM analysis provides a direct visual evidence of the spherical shape of the Ag nanoseeds synthesized by us and confirms their successful formation. The TEM image depicted in Fig. 2c reveals well-defined nanoparticles which combine small (2–6 nm) and large (6–10 nm) seeds. The average diameter is equal to 3.1±0.1 nm. This size interval falls within the range suitable for the subsequent photoconversion process, thus ensuring optimal light-matter interactions and an efficient energy transfer [29].
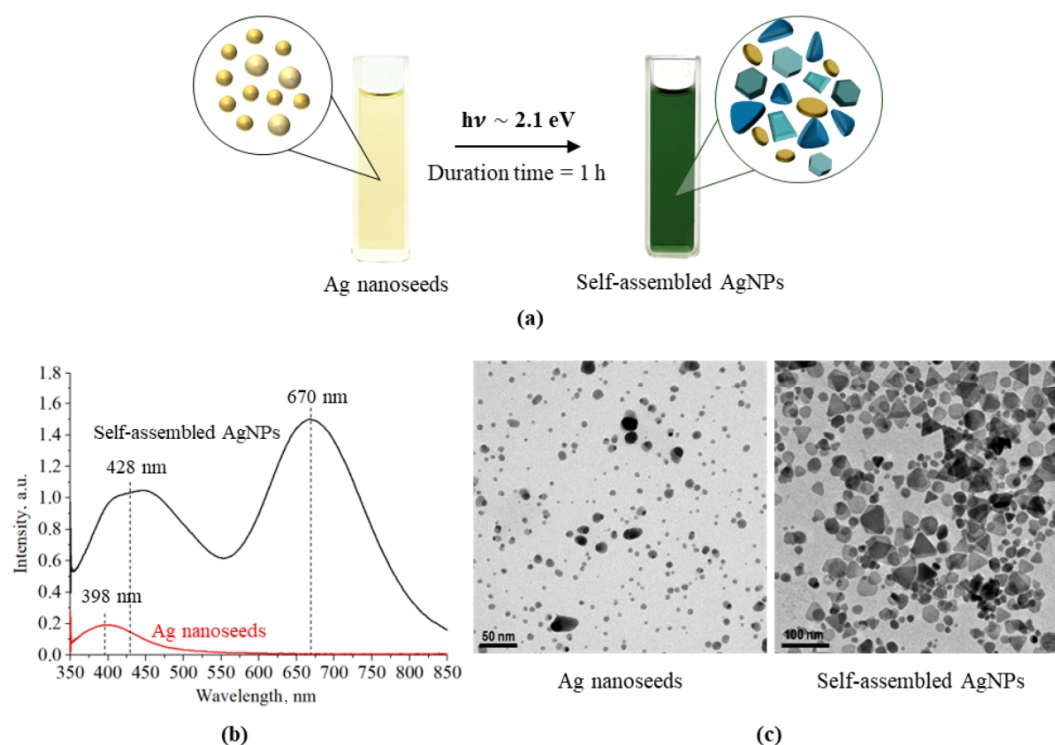

Fig. 2. The colour of colloidal Ag nanoseeds changes from bright yellow to basil green after their irradiation for 1 h with the light at the wavelength 589 nm (the photon energy 2.1 eV) (a); UV-visible absorption spectra (b) and TEM images of Ag nanoseeds and self-assembled AgNPs after their irradiation for 1 h (c).

The unique properties of the Ag nanoseeds obtained by us enable their dual functionality, which facilitates simultaneous feedstock of silver cations and promotes the reduction reactions through their plasmonic properties. Under excitation, the plasmonic seeds transfer efficiently the charge carriers (electrons or holes) to the adsorbed species, thereby driving a reduction of Ag^+ by citrate [29]. This mechanism enables a controlled growth of the AgNPs with desired morphologies, including the TSNPs, under visible-light irradiation [21].

At the specific wavelength 589 nm and the irradiance of approximately 130 mW/cm^2, the nanoseeds undergo oxidation by oxygen, resulting in generation of Ag^+ ions. Then the light-induced surface-plasmon resonance in the nanoseeds plays a crucial role in facilitating the

reduction of Ag^+ to Ag^0 through the action of citrate. This process involves the production of electrons by citrate, which actively participate in the reduction of Ag^+ under light irradiation [23, 24, 29, 30]. Additionally, the growth of the self-assembled AgNPs is guided by the citrate ions, inducing the formation of nanoplates due to their preferential binding affinity towards the (111) planes [15]. An interplay of these mechanisms enables a successful growth of the AgNPs, from the initial seeds to the formation of the TSNPs.

After 1 h of irradiation, the Ag nanoseeds undergo a transformation into the Ag nanoplates with various morphologies, resulting in a significant colour change from bright yellow to a basil green hue, as depicted in Fig. 2a. This transformation is confirmed further by the UV-visible spectra presented in Fig. 2b. Disappearance of the surface-plasmon resonance peak at approximately 398 nm and emergence of a dominant absorption peak at 670 nm provide a strong evidence of the shape transformation occurring with the nanoplates, which corresponds to an in-plane dipole plasmon resonance [31]. Additionally, a weaker and broader absorption band around 428 nm is observed. It can be attributed to an out-of-plane dipole plasmon resonance, thus indicating a presence of the large-sized spherical AgNPs mixed with the circular nanoplates [31, 32]. These results are consistent with the TEM data.

The TEM images of the resulting AgNPs (see the right-hand panel in Fig. 2c) reveal a diverse range of highly anisotropic structures. These structures include the spherical nanoparticles with the average diameter 17.0±0.6 nm (19% of all the particles), the circular nanoplates with the average diameter 28.2±1.4 nm and the thickness 9.4±0.6 nm (12% of the particles), the hexagonal nanoplates with the average edge length 30.7±1.3 nm and the thickness 11.7±0.3 nm (11% of the particles), the trapezoid nanoplates with the average edge length 16.0±1.3 nm and the thickness 6.2±0.8 nm (10% of the particles), and the triangular nanoplates with the average edge length 30.0±1.6 nm and the thickness 12.6±0.2 nm (48% of the particles).

3.2. Comparison of SERS activities of TSNPs separated at different centrifugation times

To achieve efficient separation of the TSNPs for the SERS measurements, we have subjected the colloidal solution composed predominantly of nanoplates with different morphologies to centrifugation. This has been done in order to minimize the presence of the other morphologies and retain predominantly the TSNPs, thus ensuring a high SERS activity. The centrifugation times are equal to 5, 10, 15, and 20 min, with the speed amounting to 14000 rpm.
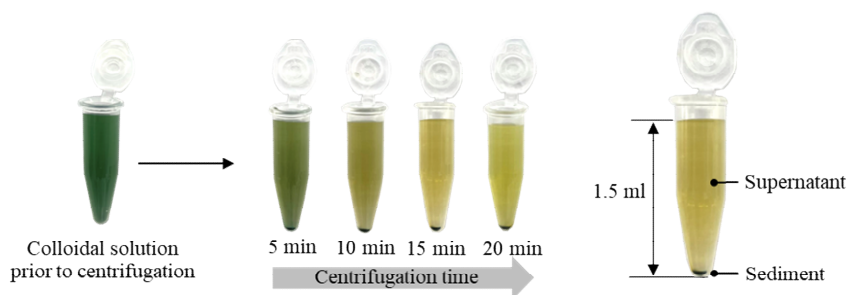

Fig. 3. Images of two-layer aqueous structures composed of supernatant and sediment phases, as taken after centrifugations with different durations (see the legend).

As depicted in Fig. 3, the phase separation begins from 5 min. A more distinct separation into two different layers is observed with increasing centrifugation time. This is visually confirmed by the colour division in the two layers. Here the supernatant phase appears to be yellow, while the sediment forms a concentrated dark blue solid-like deposit at the bottom of a microcentrifuge tube.

After that, the supernatant phase in each tube has been carefully separated, while the sediment phase has been thoroughly re-suspended in 9 mL of deionized water, thus ensuring no intermixing. The resulting supernatant and sediment phases can be visually seen in Fig. 4, which implies distinct phases obtained at different centrifugation times.
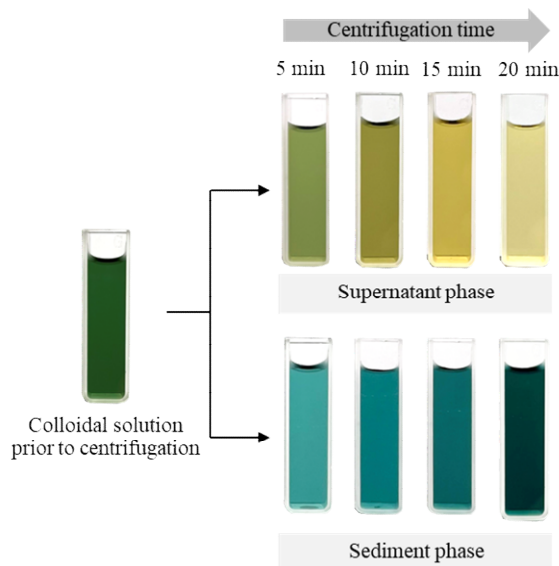

Fig. 4. Supernatant and sediment phases obtained at different centrifugation times after careful separation and re-suspension.
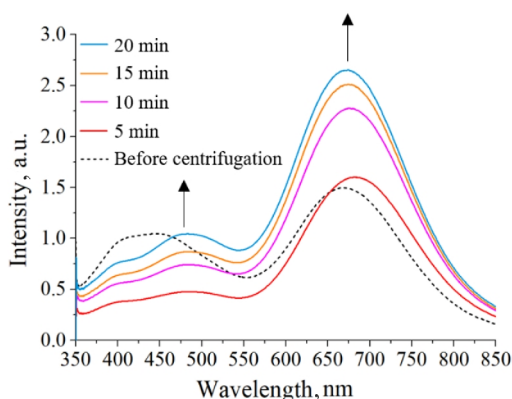

Fig. 5. UV-visible absorption spectra of colloidal AgNPs obtained before centrifugation and the same spectra of sediment-phase suspension obtained after centrifugation at different durations (see the legend).

The efficiency of the separation has been further assessed through the UV-visible spectroscopy and the TEM analysis. The UV-visible spectra shown in Fig. 5 reveal the absorbance and plasmonic characteristics of the nanoparticles and enable a comprehensive comparison of their optical properties before and after the centrifugation process is performed. After centrifugation for 5 min, the spherical nanoparticles are removed, resulting in a notable absence of broadening in the absorption band located around 428 nm. Instead, two small humps centred around 400 and 480 nm are observed, which can be assigned to the out-of-plane dipole plasmon resonance of the circular nanoplates, albeit in smaller quantities. Moreover, the main surface-plasmon resonance peak at

670 nm reveals a redshift towards 683 nm, which implies a contribution into the in-plane dipole plasmon resonance and indicates a presence of the TSNPs [33]. The peaks centred at 400, 480 and 683 nm increase with increasing centrifugation time. In particular, this refers to the peak located at 683 nm, which displays a higher and broader full width at half maximum. This observation suggests a higher amount and broader size distribution of the TSNPs due to larger gravitational forces exerted during a longer centrifugation process. Importantly, these results conform well to the TEM images presented in Fig. 6. These images show that, after centrifugation for 5, 10, 15 and 20 min, the TSNPs with the average edge length 31.1±4.8 nm account respectively for ~ 28, 58, 75 and 87% of the enriched population. Moreover, we observe enrichment with the circular, hexagonal and triangular nanoplates under these conditions, if compared to the initial nanoplate population observed before centrifugation.
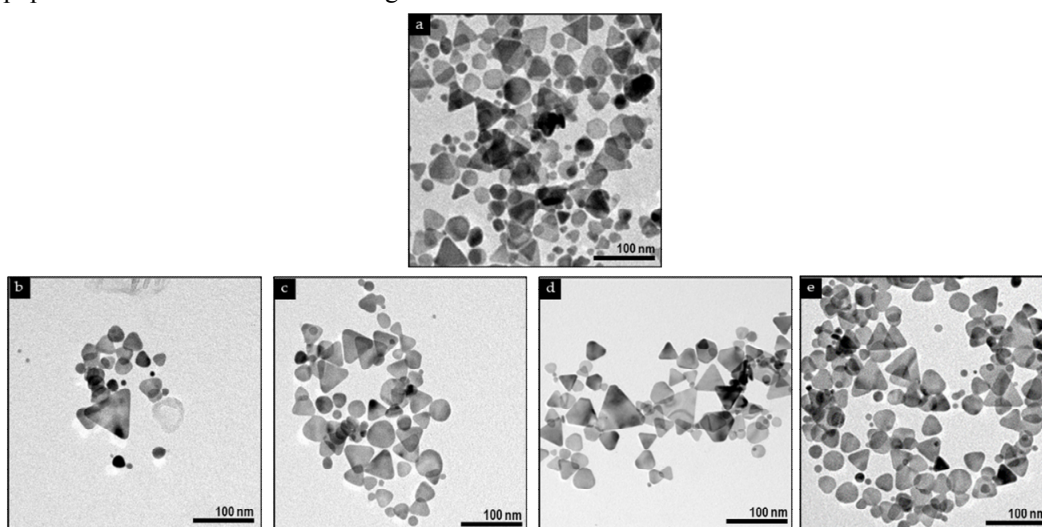

Fig. 6. Representative TEM images of AgNPs before centrifugation (a) and AgNPs in the sediment phase obtained after centrifugation for 5 (b), 10 (c), 15 (d), and 20 min (e).

Now we wish to select the optimal condition for the centrifuge-based separation process and achieve the highest enhancement in the SERS activity. For this aim, we employ the colloidal AgNPs obtained before centrifugation and the separated AgNPs obtained at different centrifugation times as colloidal SERS-active substrates, in order to amplify the Raman signal of 10^{-4} M R6G. Here our custom-designed 3D-printed liquid chamber has served as a sample holder.

Typically, several characteristic Raman shift bands can be observed in the R6G solution with the concentrations higher than 10^{-3} M even if no SERS technique is applied. Prominent Raman-shift bands are typically observed around 1362 and 1510 cm^{-1}. They represent a C–C stretching vibrations in a xanthene ring. Another notable Raman-shift band can be observed around 1651 cm^{-1}, which corresponds to a C=C stretching vibration in this ring. Additionally, a significant Raman-shift band appears around 1182 cm^{-1}, which is associated with a C–H in-plane bending vibration in the xanthene ring. Finally, weak Raman-shift bands are observed around 773 and 1311 cm^{-1}. They can be attributed to a C–H out-of-plane bending vibration and a hybrid mode, respectively [34–37].

It is evident from Fig. 7 that the characteristic Raman bands of R6G alone (under condition of no AgNPs) are too weak to be observed. However, the Raman signals become detectable when all the SERS-active substrates are utilized. The intensities of different Raman signals, in particular that of the strong primary peak located at 1510 cm^{-1}, have been used to calculate the estimated

enhancement factor *EF*. This has been done by comparing the SERS intensity (I_{SERS}) with the normal Raman intensity (I_{Raman}) according to the relation $EF = I_{SERS}/I_{Raman}$ [17, 23]. We have found that the AgNPs before centrifugation reveal the enhancement factor $EF = 492$, while centrifugation leads to higher enhancement factors. In particular, we have $EF = 739, 1003, 1343$ and 733 in the cases when the AgNPs separated respectively at the centrifugation times 5, 10, 15 and 20 min are taken as SERS-active substrates.
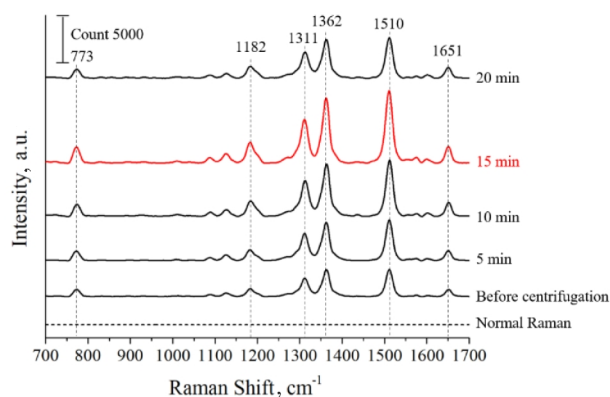

Fig. 7. A normal Raman spectrum measured for the 10^{-4} M R6G solution and SERS spectra for the same solution amplified using the AgNPs, as measured before centrifugation and at centrifugation times indicated in the legend.

The reason why the colloidal AgNPs separated at the speed 14000 rpm for 15 min yield the highest enhancement factor, if compared to the other conditions, is disappearance of the spherical nanoparticles. This results in an optimal proportion of the triangular (74%), hexagonal (20%) and circular (6%) nanoplates. These different nanoparticle shapes in the optimal quantities can reveal varying degrees of the localized surface-plasmon resonance, which potentially leads to a strong electromagnetic-field enhancement and a notable SERS-signal amplification.

3.3. Efficiency of TSNPs for a trace-level detection based on SERS

In this section, we present the experimental results and their analysis, which highlight the enhanced sensitivity and detection capabilities of the colloidal AgNPs separated under centrifugation for 15 min for R6G in a dilution series. The separated nanoparticles include predominantly the TSNPs, with smaller proportioni of hexagonal and circular nanoplates. Our findings emphasize potential applications of the TSNPs as highly efficient SERS-active substrates for a trace-level detection and open up new possibilities in such fields as sensing, diagnostics and environmental monitoring.

The spectral results depicted in Fig. 8 provide a compelling evidence of the enhanced sensitivity achieved with the separated AgNPs. It is notable that the limit of detection for the case of R6G decreases to an impressive value, 10^{-12} M. This demonstrates a remarkable capability of the TSNPs for amplifying Raman signals of R6G, even at its extremely low concentrations. This exceptional sensitivity enables one to detect R6G even at trace levels, thus making our approach promising for ultrasensitive analytical applications.

Furthermore, a linear relationship between the R6G concentration and the Raman-peak intensity increases the reliability of the SERS technique, which is based upon the colloidal AgNPs separated under centrifugation for 15 min. The correlation between the two variables is highly significant, as indicated by the R^2 value exceeding 0.99 (see Fig. 8c). This high correlation

coefficient demonstrates high consistency and reproducibility of the SERS measurements. As a result, our colloidal AgNPs can serve as robust and reliable SERS-active substrates.
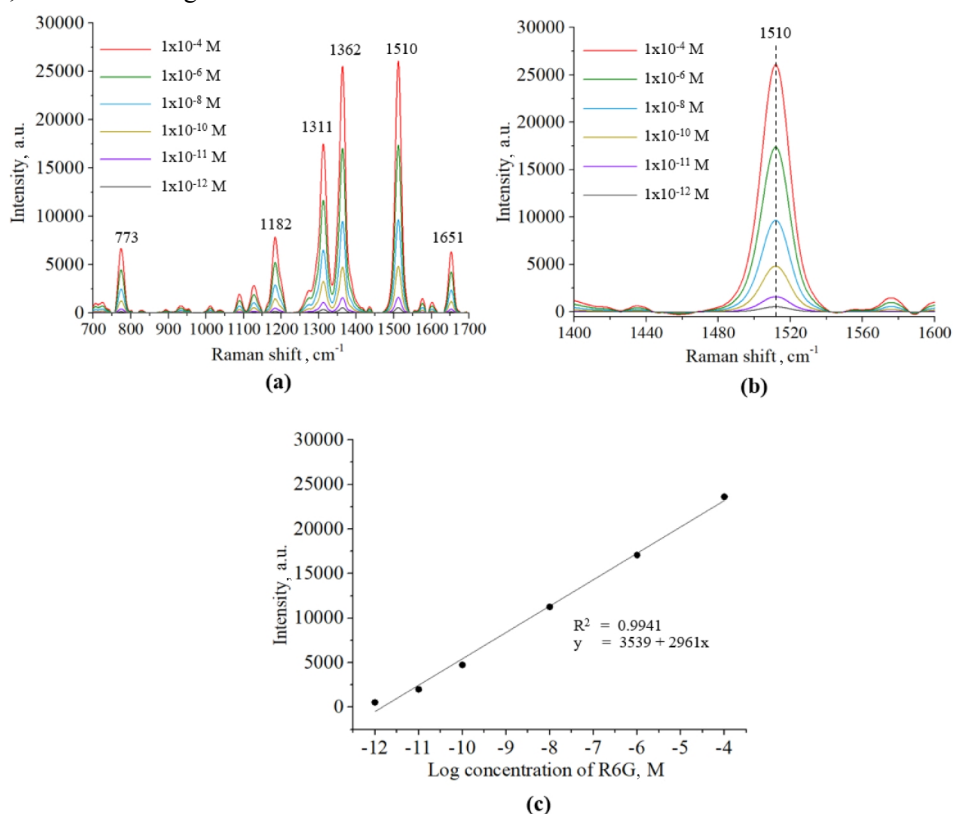

Fig. 8. (a) SERS spectra of R6G with the concentrations ranging from 10^{-12} to 10^{-4} M (see the legend), as obtained for the colloidal AgNPs (separated during 15-min centrifugation) as a SERS-active substrate; (b) a zoomed-in region (1400–1600 cm^{-1}) of the above SERS spectra; (c) a calibration curve showing logarithmic relationship between the SERS intensity detected at 1510 cm^{-1} and the R6G concentration.

4. Conclusions

We have successfully synthesized the TSNPs with the photochemical process and implemented their centrifugation-based separation in order to boost the SERS performance. The optimization of the synthesis parameters and the separation process allow us to isolate the TSNPs with a minimal presence of the other nanoparticle morphologies. The TSNPs separated in this way, which are mixed with the hexagonal and circular nanoplates in smaller proportions, reveal an exceptional SERS sensitivity. It can be characterized by the detection limit for R6G as low as 10^{-12} M. The linear relationship observed between the R6G concentration and the Raman-peak intensity emphasizes further a great potential of the SERS technique based on the separated TSNPs.

In other words, our study reveals a reliable and reproducible approach for the SERS measurements and demonstrates that the TSNPs can represent promising and highly efficient SERS-active substrates for the trace-level detection of substances in various fields. Future researches along this direction can explore a potential of the TSNPs for the other analytes and further clarify the conditions of optimized synthesis and separation still greater enhancement of the SERS performance. The findings of our study contribute significantly to the advances of the SERS technique and provide valuable insights into the development of highly sensitive and selective detection techniques for diverse scientific and technological applications.

References

1. Jones R R, Hooper D C, Zhang L, Wolverson D and Valev V K, 2019. Raman techniques: fundamentals and frontiers. Nanoscale Res. Lett. **14**: 231.
2. Pence I and Mahadevan-Jansen A, 2016. Clinical instrumentation and applications of Raman spectroscopy. Chem. Soc. Rev. **45**: 1958–1979.
3. Yuan K, Jurado-Sánchez B and Escarpa A, 2022. Nanomaterials meet surface-enhanced Raman scattering towards enhanced clinical diagnosis: a review. J. Nanobiotechnol. **20**: 537.
4. Zhao L, Gu W, Zhang C, Shi X and Xian Y, 2016. In situ regulation nanoarchitecture of Au nanoparticles/reduced graphene oxide colloid for sensitive and selective SERS detection of lead ions. J. Colloid Interface Sci. **465**: 279–285.
5. Muehlethaler C, Leona M and Lombardi J R, 2016. Review of surface enhanced Raman scattering applications in forensic science. Analyt. Chem. **88**: 152–169.
6. Petryayeva E and Krull U J, 2011. Localized surface plasmon resonance: nanostructures, bioassays and biosensing – a review. Anal. Chim. Acta. **706**: 8–24.
7. Pustovit V N and Shahbazyan T V, 2005. Quantum-size effects in SERS from noble-metal nanoparticles. Microelectron. J. **36**: 559–563.
8. Cong S, Liu X, Jiang Y, Zhang W and Zhao Z, 2020. Surface enhanced Raman scattering revealed by interfacial charge–transfer transitions. Innovation (Camb). **1**: 100051.
9. Chen T, Wang H, Chen G, Wang Y, Feng Y, Teo WS, Wu T and Chen H, 2010. Hotspot-induced transformation of surface-enhanced Raman scattering fingerprints. ACS Nano. **4**: 3087–3094.
10. Krajczewski J, Joubert V and Kudelski A, 2014. Light-induced transformation of citrate stabilized silver nanoparticles: photochemical method of increase of SERS activity of silver colloids. Colloids Surf. A: Physicochem. Eng. Asp. **456**: 41–48.
11. Puente C, Pineda Aguilar N, Gómez I and López I, 2023. Morphology effect of photoconverted silver nanoparticles on the performance of surface-enhanced Raman spectroscopy substrates. ACS Omega. **8**: 12630–12635.
12. Le Ru E C and Etchegoin P G. Principles of Surface-Enhanced Raman Spectroscopy. Elsevier: Oxford, 2008.
13. Zannotti M, Rossi A and Giovannetti R, 2020. SERS activity of silver nanosphere, triangular nanoplates, hexagonal nanoplates and quasi-spherical nanoparticles: effect of shape and morphology. Coatings. **10**: 288.
14. Estrada-Mendoza T A, Willett D and Chumanov G, 2020. Light absorption and scattering by silver/silver sulfide hybrid nanoparticles. J. Phys. Chem. C. **124**: 27024–27031.
15. Pastoriza-Santos I and Liz-Marzán L M, 2008. Colloidal silver nanoplates. State of the art and future challenges. J. Mater. Chem. **18**: 1724–1737.

16. Jana D, Mandal A and De G, 2012. High Raman enhancing shape-tunable ag nanoplates in alumina: a reliable and efficient SERS technique. ACS Appl. Mater Interfaces. **4**: 3330–3334.

17. Tiwari V S, Oleg T, Darbha G K, Hardy W, Singh J P and Ray P C, 2007. Non-resonance SERS effects of silver colloids with different shapes. Chem. Phys. Lett. **446**: 77–82.

18. Iravani S, Korbekandi H, Mirmohammadi S V and Zolfaghari B, 2014. Synthesis of silver nanoparticles: chemical, physical and biological methods. Res. Pharm. Sci. **9**: 385–406.

19. Tanimoto H, Ohmura S and Maeda Y, 2012. Size-selective formation of hexagonal silver nanoprisms in silver citrate solution by monochromatic-visible-light irradiation. J. Phys. Chem. C. **116**: 15819–15825.

20. Tang B, Sun L, Li J, Zhang M and Wang X, 2015. Sunlight-driven synthesis of anisotropic silver nanoparticles. J. Chem. Eng. **260**: 99–106.

21. Stamplecoskie K G and Scaiano J C, 2010. Light emitting diode irradiation can control the morphology and optical properties of silver nanoparticles. J. Amer. Chem. Soc. **132**: 1825–1827.

22. Saade J and Araújo C B, 2014. Synthesis of silver nanoprisms: a photochemical approach using light emission diodes. Mater. Chem. Phys. **148**: 1184–1193.

23. Nhung N T H, Dat N T, Thi C M and Viet P V, 2020. Fast and simple synthesis of triangular silver nanoparticles under the assistance of light. Colloids Surf. A: Physicochem. Eng. Asp. **594** (2020): 124659.

24. Xue B, Wang D, Zuo J, Kong X, Zhang Y, Liu X, Tu L, Chang Y, Li C, Wu F, Zeng Q, Zhao H, Zhao H and Zhang H, 2015. Towards high quality triangular silver nanoprisms: improved synthesis, six-tip based hot spots and ultra-high local surface plasmon resonance sensitivity. Nanoscale. **7**: 8048–8057.

25. Millstone J E, Hurst S J, Métraux G S, Cutler J I and Mirkin C A, 2009. Colloidal gold and silver triangular nanoprisms. Small. **5**: 646–6464.

26. Haitao W, Xiaoqiang C, Weiming G, Xianliang Z, Hetong Z, Tianyu X and Weitao Z, 2016. Synthesis of silver nanoprisms and nanodecahedra for plasmonic modulating surface-enhanced Raman scattering. J. Nanosci. Nanotechnol. **16**: 6829–6836.

27. Wang H, Cui X, Guan W, Zheng X, Zhao H, Wang Z, Wang Q, Xue T, Liu C, Singh DJ and Zheng W, 2014. Kinetic effects in the photomediated synthesis of silver nanodecahedra and nanoprisms: combined effect of wavelength and temperature. Nanoscale. **6**: 7295–7302.

28. Swarnavalli G C J, Joseph V, Kannappan V and Roopsingh D, 2011. A simple approach to the synthesis of hexagonal-shaped silver nanoplates. J. Nanomater. **2011**: 1–5.

29. Xue C, Métraux G S, Millstone J E and Mirkin C A, 2008. Mechanistic study of photomediated triangular silver nanoprism growth. J. Amer. Chem. Soc. **130**: 8337–8344.

30. Stamplecoskie K G, Scaiano J C, Tiwari V S and Anis H, 2011. Optimal size of silver nanoparticles for surface-enhanced Raman spectroscopy. J. Phys. Chem. C. **115**: 1403–1409.

31. Brioude A and Pileni M P, 2005. Silver nanodisks: optical properties study using the discrete dipole approximation method. J. Phys. Chem. B. **109**: 23371–23377.

32. Bartlett T R, Sokolov S V, Plowman B J, Young N P and Compton R G, 2016. Tracking of photochemical Ostwald ripening of nanoparticles through voltammetric atom counting. Nanoscale. **8**: 16075–16530.

33. Kelly K L, Coronado E, Zhao L L and Schatz G C, 2003. The optical properties of metal nanoparticles: the influence of size, shape, and dielectric environment. J. Phys. Chem. B. **107**: 668–677.

34. Watanabe H, Hayazawa N, Inouye Y and Kawata S, 2005. DFT vibrational calculations of rhodamine 6G adsorbed on silver: analysis of tip-enhanced Raman spectroscopy. J. Phys. Chem. B. **109**: 5012–5020.

35. Hildebrandt P and Stockburger M, 1984. Surface-enhanced resonance Raman spectroscopy of rhodamine 6G adsorbed on colloidal silver. J. Phys. Chem. **88**: 5935–5944.

36. Zhong F, Wu Z, Guo J and Jia D, 2018. Porous silicon photonic crystals coated with Ag nanoparticles as efficient substrates for detecting trace explosives using SERS. Nanomater. **8**: 872.

37. He X N, Gao Y, Mahjouri-Samani M, Black P N, Allen J, Mitchell M, Xiong W, Zhou Y S, Jiang L and Lu Y F, 2012. Surface-enhanced Raman spectroscopy using gold-coated horizontally aligned carbon nanotubes. Nanotechnol. **23**: 205702.

Анотація. *Ми синтезували та розділили трикутні срібні нанопластини (ТСНП) із суміші колоїдних наночастинок срібла різних форм і розмірів із метою виготовлення підкладок для поверхнево-підсиленого комбінаційного розсіювання (ППКР). ТСНП успішно синтезовано за допомогою фотохімічного процесу за участю нанозерен Ag. Це підтверджено методом ультрафіолетової та видимої спектроскопії, а також даними трансмісійної електронної мікроскопії. Методи розділення на основі центрифугування використано для ізоляції ТСНП і мінімізації інших морфологій наночастинок, що забезпечило високу ефективність ППКР. Відокремлені ТСНП виявляють дуже високу чутливість, із межею виявлення, що складає 10^{-12} М для випадку молекул родаміну 6G. Лінійний зв'язок між концентрацією родаміну 6G та інтенсивністю раманівського піку демонструє значний потенціал нашої методики ППКР. Отже, наше дослідження поєднало успішний синтез і розділення ТСНП із демонстрацією їхньої ефективної ППКР. Останнє пропонує нові можливості для ультрачутливого виявлення слідів речовин. Ці результати сприятимуть розробці надійних вимірювань ППКР і прогресові в галузі методів зондування на основі наноматеріалів.*

Ключові слова*: трикутні срібні нанопластини, розділення на основі центрифугування, поверхнево-підсилене комбінаційне розсіювання, фотохімічний синтез*